Monthly Notices
of the
ROYAL ASTRONOMICAL SOCIETY

MNRAS **448,** 1779–1788 (2015) doi:10.1093/mnras/stv069

Hubble Space Telescope observations of the *Kepler*-field cluster NGC 6819 – I. The bottom of the white dwarf cooling sequence⋆

L. R. Bedin,[1]† M. Salaris,[2] J. Anderson,[3] S. Cassisi,[4] A. P. Milone,[5] G. Piotto,[1,6] I. R. King[7] and P. Bergeron[8]

[1]*INAF-Osservatorio Astronomico di Padova, Vicolo dell'Osservatorio 5, I-35122 Padova, Italy*
[2]*Astrophysics Research Institute, Liverpool John Moores University, 146 Brownlow Hill, Liverpool L3 5RF, UK*
[3]*Space Telescope Science Institute, 3800 San Martin Drive, Baltimore, MD 21218, USA*
[4]*INAF-Osservatorio Astronomico di Collurania, via M. Maggini, I-64100 Teramo, Italy*
[5]*Research School of Astronomy and Astrophysics, The Australian National University, Cotter Road, Weston, ACT 2611, Australia*
[6]*Dipartimento di Fisica e Astronomia 'Galileo Galilei', Università di Padova, Vicolo dell'Osservatorio 3, I-35122 Padova, Italy*
[7]*Department of Astronomy, University of Washington, Box 351580, Seattle, WA 98195-1580, USA*
[8]*Département de Physique, Université de Montréal, C.P. 6128, Succ. Centre-Ville, Montréal, Québec H3C 3J7, Canada*

Accepted 2015 January 12. Received 2015 January 9; in original form 2014 November 27

ABSTRACT

We use *Hubble Space Telescope* (*HST*) to reach the end of the white dwarf (WD) cooling sequence (CS) in the solar-metallicity open cluster NGC 6819. Our photometry and completeness tests show a sharp drop in the number of WDs along the CS at magnitudes fainter than $m_{\rm F606W} = 26.050 \pm 0.075$. This implies an age of 2.25 ± 0.20 Gyr, consistent with the age of 2.25 ± 0.30 Gyr obtained from fits to the main-sequence turn-off. The use of different WD cooling models and initial–final-mass relations have a minor impact the WD age estimate, at the level of ∼0.1 Gyr. As an important by-product of this investigation we also release, in electronic format, both the catalogue of all the detected sources and the atlases of the region (in two filters). Indeed, this patch of sky studied by *HST* (of size ∼70 arcmin^2) is entirely within the main *Kepler*-mission field, so the high-resolution images and deep catalogues will be particularly useful.

Key words: open clusters and associations: individual: NGC 6819 – white dwarfs.

1 INTRODUCTION

During the last few decades, both observations and theory have improved to a level that has made it possible to employ white dwarf (WD) stars for estimating ages of stellar populations in the solar neighbourhood (i.e. Winget et al. 1987; García-Berro et al. 1988; Oswalt et al. 1996), open (i.e. Richer et al. 1998; von Hippel 2005; Bedin et al. 2008a, 2010) and globular (i.e. Hansen et al. 2004, 2007; Bedin et al. 2009) clusters.

Methods to determine stellar population ages from their WD cooling sequences (CSs) are usually based on the comparison of the observed WD luminosity function (LF – star counts as a function of magnitude) with theoretical ones calculated from WD isochrones. When considering star clusters, owing to the single (and finite) age of their stars, the more massive WDs formed from higher mass short-lived progenitors pile up at the bottom of the CS, producing a turn to the blue (a turn towards lower radii) in the isochrones. At old ages, when the WD $T_{\rm eff}$ decreases below ≈5000 K, the contribution by collision-induced absorption of molecular hydrogen (Hansen 1998) to the opacity in the atmospheres reduces the infrared flux and increase the flux at shorter wavelengths. This produces a turn to the blue of the colours of individual cooling tracks, that enhances the blue excursion at the bottom of old WD isochrones. The existence of a minimum WD luminosity due to the cluster finite age, together with the accumulation of WDs of different masses and a general increase of WD cooling times with decreasing luminosity (at least before the onset of Debye cooling) translates into a peak and cut-off in the LF. Comparisons of observed and predicted absolute magnitudes of the WD LF cut-off provides the population age.

The discovery of a second, brighter peak in the WD LF of the metal-rich open cluster NGC 6791 (see Bedin et al. 2005b, 2008a,b, for the discovery and possible interpretations) has raised questions about our understanding of the CS in simple systems like open clusters, and their use for age dating of stellar populations. In particular, this bright peak has been interpreted by Kalirai et al. (2007) as due

⋆ Based on observations with the NASA/ESA *Hubble Space Telescope*, obtained at the Space Telescope Science Institute, which is operated by AURA, Inc., under NASA contract NAS 5-26555, under GO-11688 and GO-12669.

† E-mail: luigi.bedin@oapd.inaf.it

© 2015 The Authors
Published by Oxford University Press on behalf of the Royal Astronomical Society

to a population of massive He-core WDs, whilst Bedin et al. (2008b) have explained it in terms of a sizeable population of WD+WD binaries. As for the fainter peak – expected to be the *real* age indicator– the age obtained from standard WD models is in conflict (∼2 Gyr younger) with that derived from the cluster main-sequence (MS) turn-off (TO), and the age later obtained from the cluster eclipsing binaries studied by Brogaard et al. (2012). This discrepancy has led to a detailed re-evaluation of the effect of diffusion of ^{22}Ne in the CO core before crystallization sets in (e.g. Bravo et al. 1992, Deloye & Bildsten 2002). As shown by García-Berro et al. (2010, 2011) with full evolutionary calculations, at the old age and high metallicity of this cluster (about twice solar), the extra energy contributed by Ne-diffusion in the liquid phase slows down substantially the cooling of the models and can bring into agreement WD, TO and eclipsing binary ages.

This result highlights very clearly the need for further observations, and the importance of studying WD ages in comparison with TO estimates in individual clusters. As WDs lie in one of the least-explored regions of the colour–magnitude diagram (CMD), we are carrying out a campaign to find out whether the case of NGC 6791 is unique or whether other clusters with similar WD CSs might exist. Our purpose is to extend our knowledge of the dependence of WD LFs on cluster age and metallicity. So far, we have investigated two other open clusters: NGC 2158 from space (Bedin et al. 2010), and M 67 from the ground (Bellini et al. 2010); both of them show canonical WD CSs (hence LFs).

The aim of this work is to investigate the WD CS of another open cluster, NGC 6819, that is within the *Kepler*-mission field. NGC 6819 has solar metallicity (Bragaglia et al. 2001), is about a fourth as old as NGC 6791 (Anthony-Twarog, Deliyannis & Twarog 2014), and somewhat less massive (as can be inferred from their images in the Digital Sky Survey).

Section 2 will describe our observations and WD selection, whilst Section 3 presents the theoretical analysis of the WD LF. Sections 4 and 5 discuss our proper motion analysis and present the electronic material we make publicly available. Conclusions close the paper.

2 OBSERVATIONS, MEASUREMENTS AND SELECTIONS

All data presented here were collected with two different instruments at the focus of the *Hubble Space Telescope* (*HST*) under two programmes taken at different epochs, GO-11688 and GO-12669 (on both PI: Bedin).

For the first epoch (GO-11688), eight orbits were allocated in two filters during 2009 October, while the second epoch (four orbits) was in 2012 October and used only the redder of the two filters. As primary instrument, the Ultraviolet–Visible (UVIS) channel of the Wide Field Camera 3 (WFC3) gathered images in four contiguous fields (each 162 arcsec × 162 arcsec) organized in a 2 × 2 array centred on the core of NGC 6819. The same number of fields were also observed in parallel, with the Wide Field Channel (WFC) of the Advanced Camera for Surveys (ACS, each 202 arcsec × 202 arcsec), which is located in the *HST* focal plane at about 6 arcmin from UVIS, and with the detector axes oriented at ∼45° from the WFC3 axes. Thus, the primary plus parallel exposures covered a total of about 70 arcmin^2 in NGC 6819 (see the top-left panel of Fig. 1).

All collected images were taken in the filters F606W and F814W, which are the optimal choice for our scientific goals, i.e. the study of the faintest WDs in a relatively-old open cluster, and are available for both instruments (although with different zero-points and slightly different colour responses). Data were organized in one-orbit visits per filter and per field. Each orbit consists of one 10 s short and 4 × ∼ 600 s long exposures for the primary instrument, and 3 × ∼ 470 s long exposures for ACS. Within each orbit, both instruments use analogous filters. The bottom panels of Fig. 1 show a stacked image of the regions, after removal of cosmic rays and most of the artefacts.

All images were treated with the procedures described in detail by Anderson & Bedin (2010), to correct positions and fluxes for imperfections in the charge-transfer efficiency of both ACS/WFC and WFC3/UVIS. Finally, in all images, we masked-out by hand the ghosts of the brightest stars in the fields.[1]

Photometry and relative positions were obtained with the software tools described by Anderson et al. (2008). In addition to solving for positions and fluxes, we also computed two important diagnostic parameters: quality-fit and rmsSKY. The quality-fit essentially tells how well the flux distribution resembles the shape of the point spread function (defined in Anderson et al. 2008); this parameter can be very useful for eliminating the faint blue galaxies that plague studies of WDs (see Bedin et al. 2009 for detailed discussions). The sky-smoothness parameter rmsSKY is the rms deviation from the mean, for the pixels in an annulus from 3.5 to 8 pixels from each source. As discussed in Bedin et al. (2008a), rmsSKY is invaluable in measuring a more effective completeness than has been used in most previous studies.

The photometry was calibrated to the Vega-mag system following the procedures given in Bedin et al. (2005a), and using the most-updated encircled energy curves and zero-points.[2] In the following, we will use for these calibrated magnitudes the symbols $m_{\rm F606W}$ and $m_{\rm F814W}$. The absolute accuracy of the calibration should be good to about 0.02 mag per filter.

The ACS/WFC parallel fields, although useful to derive the present-day mass function (MF) in the outskirts of the clusters from the MS stars, are not very useful to study the WD CS, as the handful of WDs are outnumbered by the field stars and background galaxies. There are also fewer ACS/WFC images than WFC3/UVIS images, and their larger pixels size complicates the identification of true point-sources, and the measurement of proper motions. Also, there are no short exposures for the WFC images, making these data useless for studying the evolved members of NGC 6819. Nevertheless, for completeness and given the interest in this patch of sky, which falls inside the *Kepler* field, we release the catalogue and atlases for the ACS/WFC fields as well (see Section 5).

Hereafter, we will use only the WFC3/UVIS central field. In particular, the long exposures of the primary field will be used to study the WD CS of NGC 6819, while the short exposures will allow us to study the brightest and evolved cluster members. The photometry obtained from the short exposures was corrected for differential reddening as in Milone et al. (2012, see their section 3), and carefully registered to the zero-points of the long exposures using unsaturated common stars. A precision of ∼0.01 mag per filter was estimated for this operation; this means that the photometry from short and long exposures should be consistent to this level.

[1] (from WFC3 instrument handbook, section 6.5.3): the WFC3 UVIS channel exhibits three different types of optical ghosts: (a) those due to reflections between the CCD front surface and the two detector package windows; (b) those due to reflections between the window surfaces and (c) those due to reflections within the particular filter in use.

[2] http://www.stsci.edu/hst/wfc3/phot_zp_lbn; http://www.stsci.edu/hst/acs/analysis/zeropoints.

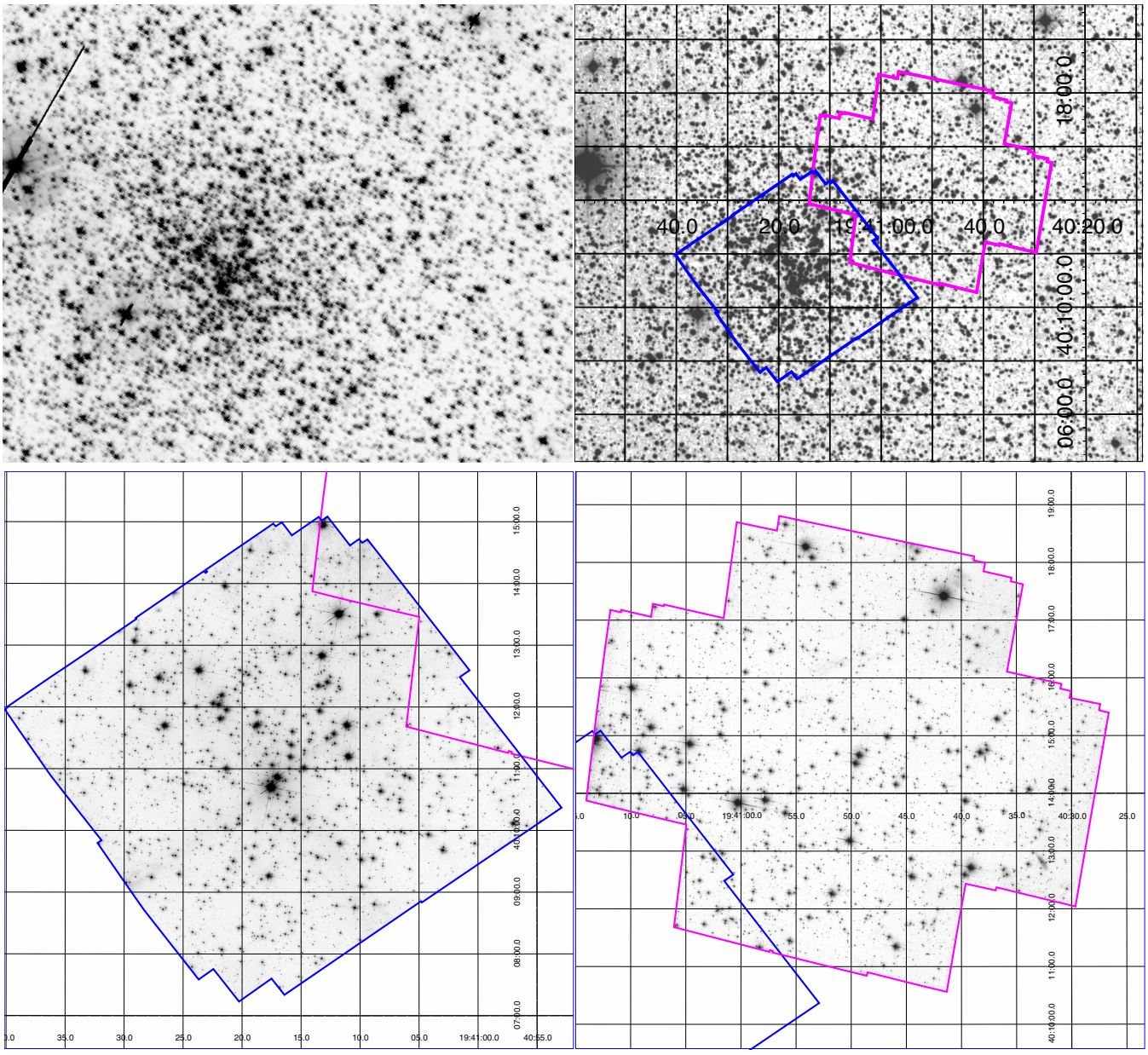

Figure 1. Top-right: overimposed on the DSS is the location of the eight primary and secondary *HST* fields employed in this work. Top-left: the same region as seen in one of the periodic full-frame images collected by the *Kepler*-mission (image: `kplr2009114174833_ffi-cal_c50.fits`). Bottom: stacked images of deep exposures in the filter F814W. On the left, we display the four primary WFC3/UVIS fields (blue outline), on the right the four parallel ASC/WFC fields (magenta outline). On both panels, we show reference grids of equatorial coordinates at J2000.0. These images are released in electronic format, as part of this work.

Artificial-star (AS) tests were performed using the procedures described by Anderson et al. (2008). We chose to cover the magnitude range $\sim 23 < m_{\rm F606W} < \sim 28.5$, with colours that placed the ASs on the WD sequence. These tests played an important role in showing us what selection criteria should be used for the real stars. The quality of our results depends very much on making a good selection, the details for which are shown in Fig. 2. (See Bedin et al. 2009, 2010, for a detailed description of the selection procedures.) Panels with unprimed labels refer to real stars, while those with primed labels refer to the ASs.

We used the AS tests to show what combinations of magnitude and quality-fit are acceptable for valid star images (panel a′), and we drew the blue lines to isolate the acceptable region. We then drew identical lines in panel (a), to separate the real stars from blends and probable galaxies. We went through similar steps for the rmsSKY parameter (panels b′ and b). This step eliminated very few stars, but is invaluable for the completeness estimate described below. Finally, we plotted CMDs and drew dividing lines in a similar way to isolate the WDs (panels c′ and c) from field objects. Thankfully, WDs occupy a relatively uncontaminated region of the CMD (Bedin et al. 2009).

As one can see from panels (a) and (a′), the shape (i.e. the quality-fit) of the objects becomes increasingly confused with the noise at magnitudes fainter than $m_{\rm F606W} \sim 26$, and therefore a few blue compact background galaxies might have fallen in the list of selected objects. However, these cannot affect the location of the drop of

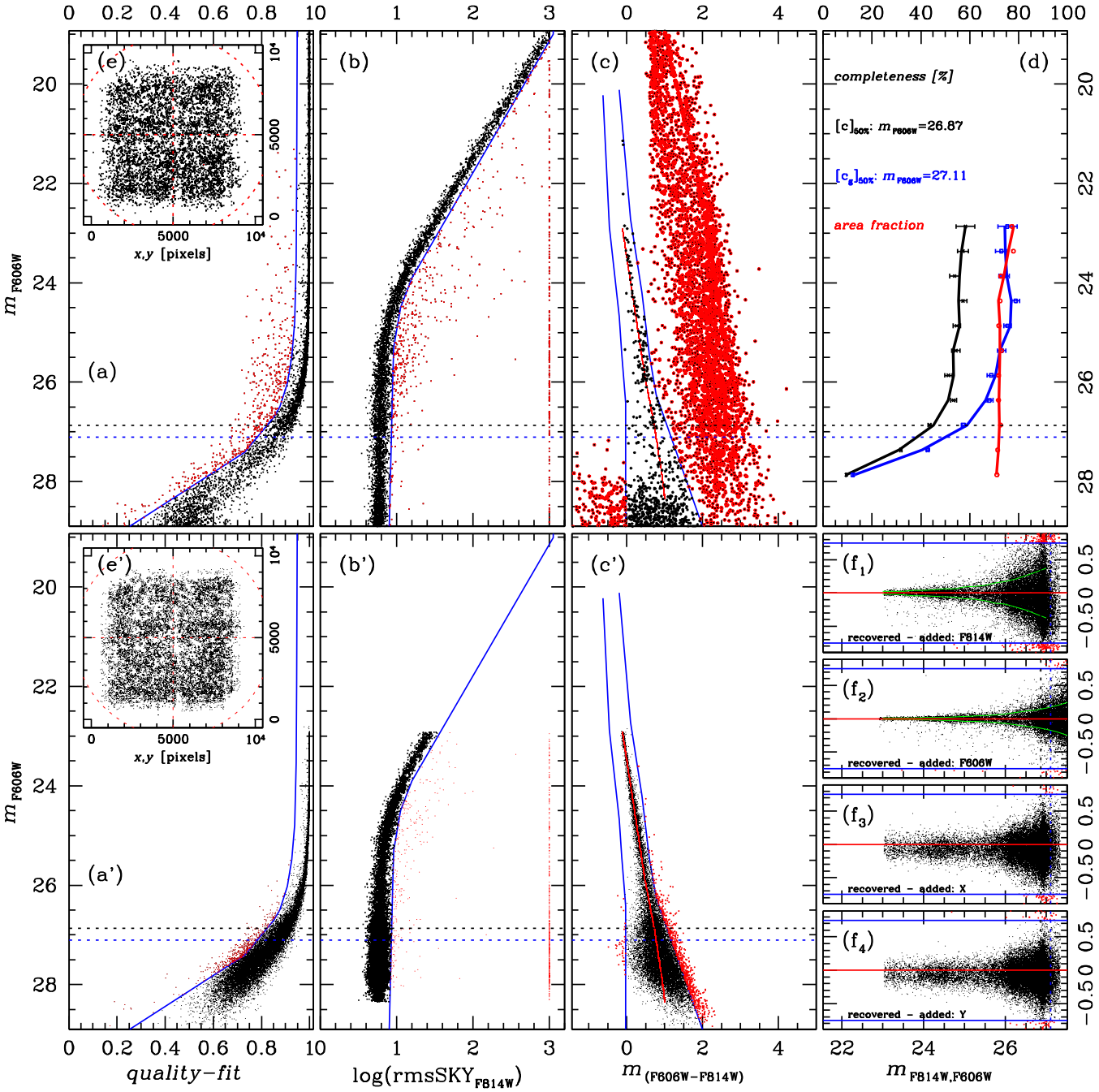

Figure 2. (a) and (a′): the parameter quality-fit as a function of magnitude, for real stars and ASs. Objects that we consider to be real stars lie to the right of the blue lines. The discarded sources are highlighted in red. [In all cases here except (d), the blue lines were drawn by hand in the lower panel and copied into the upper panel.] (b) and (b′): the parameter rmsSKY as a function of magnitude. Stars that lie on an acceptable background are located to the left of the blue lines. (c) and (c′): the CMD, with blue lines bounding the WD region. The red lines show the fiducial line along which the ASs were added. (d): black points and line show the traditional 'completeness' that ignores the rmsSKY criterion, while the blue points and line show the completeness in the regions where faint stars can be detected and measured. The red line shows the size of this measurable area in terms of fraction of total area. (e) and (e′): spatial distribution of the real and AS detections. The assumed cluster centre is indicated by the red dashed lines. Panels ($f_{1,2,3,4}$), display the recovered minus added residual biases in magnitudes and positions. The red line marks a difference equal to zero, while the blue lines mark the interval within which a star is considered recovered. The green line denotes the 68.27th percentile of the distributions.

WD star counts, which is the relevant feature studied in our work. Furthermore, the proper motions described in Section 4, confirm the WD LF cut-off magnitude.

Our final step was to deal with completeness, a concept that appears in two different contexts. (1) The observed number of WDs must be corrected for a magnitude-dependent incompleteness. (2) It is customary to choose the limiting reliable magnitude at the level where the sample is 50 per cent complete. In a star cluster, these two aims need to be treated in quite different ways. (1′) To correct for incompleteness of the WD LF, we use the traditional

ratio of AS recovered to the number inserted. (2′) For the limit to which measures of faint stars are reliable, however, the 50 per cent-completeness level needs to be chosen in a quite different way, because in a crowded star cluster more faint stars are lost in the brightness fluctuations around the bright stars, than are lost to the fluctuations of the sky background. The completeness measure that we should use to set the 50 per cent limit is therefore the recovered fraction of ASs *only* among those ASs whose value of rmsSKY, as a function of magnitude, indicates that it *was possible to recover the star*. (For a more detailed discussion, see section 4 of Bedin et al. 2008a, and for other two similar applications and further discussions see Bedin et al. 2009, 2010).

The distinction between the two completeness measures is illustrated in panel (d) of Fig. 2, where the black line shows the overall completeness, while the blue line shows the completeness statistics that take rmsSKY into account; its 50 per cent completeness level is at $m_{\rm F606W} = 27.11$, rather than 26.87 mag with the traditional statistics. To emphasize the contrast, the red line shows the fraction of the area (i.e. with low-background) in which faint stars could have been found.

3 COMPARISON WITH THEORY

As in our previous similar works on other clusters, the comparison with theory comprises the determination of an MS TO age, and the age implied by the WD LF.

BaSTI[3] scaled-solar isochrones for both WD (Salaris et al. 2010) and pre-WD (Pietrinferni et al. 2004) evolutionary phases, including MS convective-core overshooting, were used to determine both MS TO and WD ages. We considered the available BaSTI (pre-WD and WD) isochrones for [Fe/H] = +0.06, consistent with [Fe/H] = +0.09±0.03 determined spectroscopically for a sample of cluster red clump stars by Bragaglia et al. (2001 – but see Anthony-Twarog et al. 2014, for a slightly different estimates, [Fe/H] = −0.06±0.04, obtained from *uvby* Ca Hβ observations).

First, we determined the cluster distance modulus from isochrone fitting to the MS. Given that stars above the MS TO are saturated, we could not use the magnitude of the red clump and the colour of red giant branch stars as constraints. We have considered the unevolved cluster MS between $m_{\rm F606W} = 17$ (about two magnitudes below the MS TO) and 19, and derived a fiducial line by taking the mode of the $(m_{\rm F606W} - m_{\rm F814W})$ colour distribution of MS stars in 0.25 mag wide $m_{\rm F606W}$ bins. Before performing a least-square fitting of the isochrone MSs to the fiducial line, we fixed the cluster $E(B - V)$ to values between 0.10 and 0.18 mag, in steps of 0.01 mag. We explored this range following the estimate by Bragaglia et al. (2001), who used temperatures of three red clump stars derived from line excitation (a reddening-free parameter) and the appropriate theoretical spectra, to determine their intrinsic $(B - V)$ colours. Comparison with the observed colours provided $E(B - V) = 0.14\pm0.04$ (Anthony-Twarog et al. 2014 determined $E(B - V) = 0.160\pm0.007$ from *uvby* Ca Hβ observations, within the range spanned by Bragaglia et al. estimate). These $E(B - V)$ values between 0.10 and 0.18 mag were then transformed into $E(m_{\rm F606W} - m_{\rm F814W})$ and $A_{m_{\rm F606W}}$ as described by Bedin et al. (2009), and assuming $R_V = 3.1$. For each $E(m_{\rm F606W} - m_{\rm F814W})$, we finally fitted isochrones of various ages to the fiducial line. The procedure worked as follows. For a given choice of $E(B - V)$, the vertical shift required to fit the isochrones to the observed MS fiducial line provided the apparent distance modulus. This is unaffected by the isochrone age, given that we were fitting the unevolved MS. Once derived the apparent distance modulus for a given $E(B - V)$, we compared magnitude and shape of the isochrones' TO with the observed CMD, for ages varying between 1.0 and 4.0 Gyr. This comparison allowed us to both estimate the TO age and narrow down the range of reddenings consistent with the isochrones.

It turned out that for some $E(B - V)$ values (and the associated distance moduli), around the TO region the shape of the isochrone that matched the observed TO magnitude was very different from the shape of the CMD. This implied that the isochrone was too old or too young compared to the real cluster age, so that the TO magnitude had matched only on account of an inconsistent distance modulus, and hence an inconsistent reddening. Our isochrone fitting provided $E(B - V) = 0.17 \pm 0.01$, $(m - M)_0 = 11.88 \pm 0.11$ [corresponding to a distance of 2377 pc, and to $(m - M)_V = 12.41 \pm 0.12$] and an MS TO age $t_{\rm MS\,TO} = 2.25 \pm 0.30$ Gyr. The total age range was fixed by the youngest and oldest isochrones that bracketed the TO region in the observed CMD for, respectively, the shortest and largest distance moduli obtained from the MS fitting. The error on the distance modulus is an internal error of our isochrone MS-fitting method that combines in quadrature the error of the least-square fit at fixed reddening, and the effect of the error on the reddening on the least-square fit value.

The reliability of our derived distance can be assessed by comparisons with completely independent methods. Sandquist et al. (2013) obtained $(m - M)_V = 12.39 \pm 0.08$ [employing $E(B - V) = 0.12 \pm 0.01$] from the cluster eclipsing binary WOCS 23009, whilst Jeffries et al. (2013) determined $(m - M)_V = 12.44 \pm 0.07$ for the eclipsing binary WOCS 40007. Wu, Li & Hekker (2014) determined $(m - M)_0 = 11.88 \pm 0.14$ [assuming $E(B - V) = 0.14 \pm 0.04$] through the global oscillation parameters $\Delta\nu$ and $\nu_{\rm max}$ and V-band photometry of the cluster red giants.

Our isochrone-based distance estimate is in good agreement with these independent results based on completely different methods.

Regarding the age, our estimate from the MS TO agrees with $t = 2.2 \pm 0.2$ Gyr obtained by Jeffries et al. (2013) by comparing the MS mass–radius relationship of the same BaSTI isochrones used here, with the masses and radii determined for the components of the cluster eclipsing binary WOCS 23009.

The upper panel of Fig. 3 shows the result of the isochrone fits, with the two isochrones that best bracket the MS TO region, i.e. 1.95 Gyr [for $(m - M)_0 = 11.99$ and $E(B - V) = 0.18$] and 2.55 Gyr [for $(m - M)_0 = 11.77$ and $E(B - V) = 0.16$], respectively. WD isochrones (for both DA and DB objects) with the same age–distance-reddening combinations are displayed in the lower panel of the same figure. Note how the termination of the DB sequence is brighter than that for the DA WDs, contrary to the result for typical globular cluster ages, because in this regime He-envelope WDs cool down more slowly that the H-envelope counterparts (see e.g. Salaris et al. 2010). To compare WD and MS TO ages, we have used the completeness-corrected WD LF, and matched with theoretical WD LFs of varying age the observed cut-off of the star counts. The observed LF – see points with error bars in Fig. 4 – exhibits just one peak and a cut-off (at $m_{\rm F606W} = 26.050\pm0.0.075$ at its faint end, as expected for a standard cluster CS. Theoretical LFs have been calculated with the Monte Carlo (MC) technique described in Bedin et al. (2008b), employing the BaSTI WD models for both DA and DB objects, and considering a Salpeter MF for the progenitors. Our MC calculations account for the photometric error as found from the data-reduction procedure and arbitrary fractions of unresolved WD+WD binaries and DA and DB WDs. The effect of random

[3] http://www.oa-teramo.inaf.it/BASTI

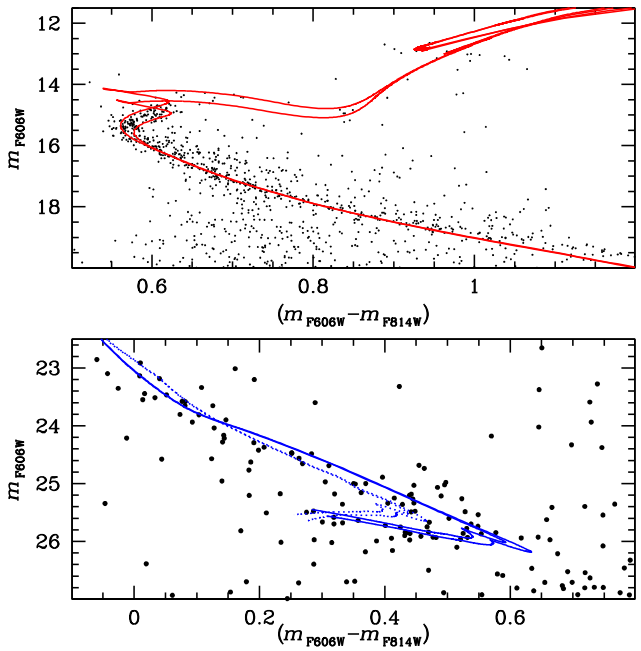

Figure 3. Upper panel: fit of theoretical isochrones [1.95 Gyr, $(m - M)_0 = 11.99$, $E(B - V) = 0.18$ and 2.55 Gyr, $(m - M)_0 = 11.77$, $E(B - V) = 0.16$] to the cluster MS in the m_{F606W}-($m_{F606W} - m_{F814W}$) CMD (see text for details). Lower panel: fit of WD isochrones to the observed CS, for the same age–distance-reddening combinations. Solid lines denote DA WDs, dotted lines DB objects.

fluctuations of the synthetic LF are minimized by using ∼100 times as many WDs as the observed sequence (which comprises about 200 objects after the completeness correction).

To give some more details, the MC code calculates the synthetic CMD of a WD population of fixed age (and initial chemical composition) by selecting first a value of the progenitor mass for a generic WD along the corresponding WD isochrone (we assume a burst of star formation with negligible age and metallicity dispersion, appropriate for open clusters), according to an initial mass function that is set to Salpeter as default choice. The corresponding mass and magnitudes of the *synthetic* WD are then determined by quadratic interpolation along the isochrone, that has been calculated assuming a WD initial–final-mass relation (IFMR; see Salaris et al. 2010 for details about the WD isochrones).[4] For the fraction of objects assumed to be in unresolved binaries, we extract randomly also a value for the ratio q between the initial mass of the companion and the mass of the WD progenitor, according to a specified statistical distribution. If the initial mass of the companion has produced a WD, we determine its mass and magnitudes as for single WDs. In case the companion is in a different evolutionary stage, we determine its magnitudes by interpolating along the pre-WD isochrone. The fluxes of the two components are then added, and the total magnitudes and colours of the composite system are computed.

We finally add the distance modulus and extinction to the magnitudes of both single and unresolved binary stars, and perturbe them randomly by using a Gaussian photometric error with the σ derived from the AS tests.

[4] WD isochrone tables for a given age and initial chemical composition provide the mass of the WD progenitor, the corresponding WD mass and the WD magnitudes in the chosen photometric filters along the CS.

A theoretical LF is then computed for the synthetic population to be compared with the observed one.

In general, the exact shape of the WD LF (and of the WD sequence in the CMD) depends on a number of parameters in addition to the cluster age, e.g. the IFMR, the MF of the progenitors, the relative fraction of the (dominant) DA and DB objects, the fraction of WD+WD binaries (and their mass distribution) and, very importantly, the dynamical evolution of the cluster, which selectively depletes the WDs according to their mass and their time of formation. Also, in open clusters, if a WD receives a sufficient velocity kick from asymmetric mass loss during its pre-WD evolution, it may become unbound (see e.g. the introduction in Williams 2004).

On one hand, this is why we are not attempting to match precisely the shape of the whole WD LF, by trying to determine simultaneously the cluster age, the precise fraction of WD+WD binaries, DB objects and the progenitor MF. These effects are difficult to disentangle using just the observed LF, and complicated by the limited statistic (total number of observed WDs, compared for example with the cases of M 4 or NGC 6791) and by a potential (although mild) residual field contamination.

On the other hand, the observed position of the WD LF cut-off, which is the primary WD age indicator, should have been affected very little by any of these parameters. In the following, we quantitatively demonstrate how all the above uncertainties, although potentially affecting the shape of the WD LF, do not alter the magnitude location of the LF cut-off.

First of all, the effect of the dynamical evolution (see Yang et al. 2013 for indications about the dynamical evolution of this cluster) should be negligible, for the following reason. The WD isochrones predict that the brighter WDs should have nearly a single mass, whereas the region of the WD LF cut-off – i.e. at the blue-turn at the bottom of the CS – is expected to be populated by objects spanning almost the whole predicted WD mass spectrum (hence the presence of a blue turn towards lower stellar radii). A mass-dependent loss mechanism due to dynamical evolution would therefore alter the number distribution of WDs around the blue-turn, but it should have no major effect on the observed location of the cut-off in the WD LF. Fig. 4 compares the completeness-corrected observed m_{F606W} WD LF (filled circles with error bars) with theoretical LFs calculated to explore some of the other effects listed above.

Panel (a) displays the theoretical LF for DA WDs (with the same number of objects as the observed candidate WDs), an age of 2.25 Gyr [$(m - M)_0 = 11.88$ and $E(B - V) = 0.17$], and two different fractions of progenitor binaries – no binaries, and 22 per cent, respectively (dotted and solid lines in the figure)– corresponding to zero, and 14 per cent WD+WD binary (supposed to be unresolved) systems on the final CS. The mass ratio q for the binary companions (the primary components are assumed to follow a Salpeter MF) was chosen with a flat distribution between 0.5 and 1.0. As discussed, e.g. in Podsiadlowski (2014), the distribution of q in binary systems is not well determined and appears to depend on the mass range. Massive binaries favour stars of comparable mass ($q \approx 1$) whilst the situation is less clear for low-mass stars, and most studies show that q is possibly consistent with a flat distribution. The 22 per cent fraction of progenitor binaries was chosen after the recent results by Milliman et al. (2014), who determined a present fraction of 22 ± 3 per cent MS binaries with period less than 10^4 d.

The unresolved systems show up in the LF at m_{F606W} between 25 and 25.2 (the variation of the star counts at fainter magnitudes is a consequence of keeping the total number of objects fixed at the observed value) about 0.75 mag brighter than the LF cut-off, as for the case of NGC 6791 (Bedin et al. 2008b). The inclusion of

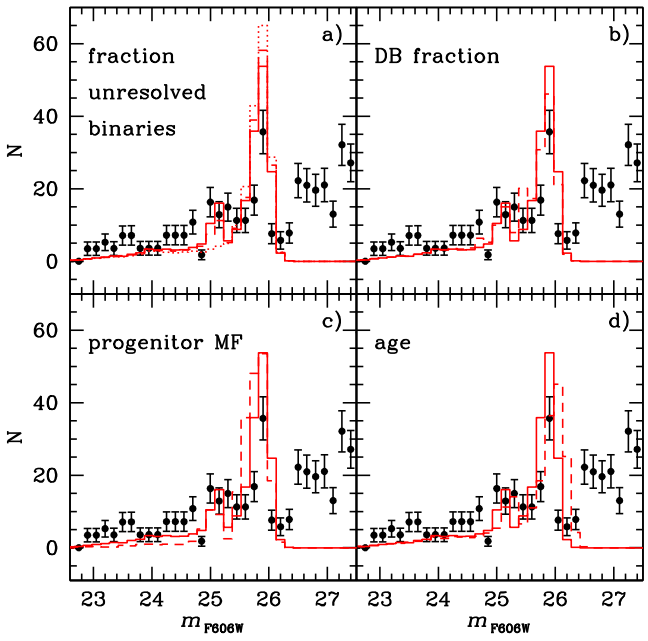

Figure 4. Comparison of the completeness-corrected observed m_{F606W} WD LF (filled circles with error bars) with theoretical 2.25 Gyr LFs, calculated with a Salpeter MF and different choices of parameters, for $E(B-V) = 0.17$ and $(m-M)_0 = 11.88$. Panel (a) displays DA LFs with no unresolved WD+WD binaries (dotted line), with a 22 per cent fraction of progenitor binaries (solid line – our reference case), and with the same fraction of progenitor binaries but a different distribution of mass ratios of the two components (dashed line – see text for details). Panel (b) displays our reference theoretical LF (solid line), and an LF with 85 per cent DA and 15 per cent DB objects, leaving everything else unchanged (dashed line). Panel (c) displays the reference LF and one calculated with a flat MF (dashed line – see text for details). Panel (d) displays our reference LF (solid line) and a 2.5 Gyr old LF, everything else being the same (dashed line).

unresolved WD+WD binaries improves the fit of the LF at those magnitudes and leaves completely unchanged the magnitude of the LF cut-off.

We have also tested the effect of changing the distribution of q by fixing the progenitor binary fraction to 22 per cent, but this time employing a flat distribution between 0.1 and 1.0. The resulting LF (dashed line) has a slightly changed shape, the local maximum between 25 and 25.2 is less pronounced, but the magnitude of the cut-off is not affected. Note how the few contaminant sources in the sample that might alter our observed WD LF below $m_{F606W} \sim 26.5$, do not affect the location of the WD LF drop-off.

Panel (b) shows the effect of including a 15 per cent fraction of DB objects (dashed line – DB isochrones are also from Salaris et al. 2010) for an age of 2.25 Gyr, and a reference 22 per cent binary progenitor fraction. Also in this case, the magnitude of the LF cut-off is unchanged, and the signature of DB WDs appears at $m_{F606W} \sim 25.5$ (the variation of the star counts at fainter magnitudes is again a consequence of keeping the total number of objects fixed). According to the observed LF, there is no room for a much higher fraction of DB objects, and actually a value close to zero would probably be a better match to the observations.

Panel (c) investigates the combined effect of varying the progenitor initial MF plus the cluster dynamical evolution that progressively depletes the lower mass (both progenitors and WDs) objects. To this purpose, we display the LF for the standard Salpeter MF (solid line – no DBs, 22 per cent of WD+WD unresolved binaries) and an LF calculated with a close to flat MF for the WD progenitors (dashed line), i.e. a power law with exponent −0.15. Progenitor masses are between ∼1.7 and ∼6.5 $M_\odot$ at our reference age of 2.25 Gyr, whilst the final WD masses range between ∼0.61 and 1.0 $M_\odot$ according to the IFMR adopted by the BaSTI WD isochrones (see Salaris et al. 2010 for details).

The comparison of the two LFs shows that the magnitude of the cut-off is unchanged, as expected. Only the overall shape is affected and the width of the peak of the theoretical LF is increased, but not the position of the drop of the star counts beyond the peak, that is the age indicator. Finally, panel (d) displays the effect of age (2.25 and 2.5 Gyr, respectively), keeping the DB fraction to zero, and the reference 22 per cent of progenitor binaries. The older LF has a fainter termination, and can be excluded by means of the comparison with the position of the observed cut-off.

After this reassessment of the solidity of the LF cut-off as age indicator, we have varied the cluster apparent distance modulus within the range established with the MS fitting and obtained a range of WD ages $t_{WD} = 2.25 \pm 0.20$ Gyr. This age range has been determined by considering all theoretical LFs that display after the peak a sharp drop in the star counts at the bin centred around $m_{F606W} = 26.05$. Note that the range is narrower than the MS TO age range, but completely consistent with $t_{MS\,TO}$. This narrower age range is due to the different sensitivity of TO and WD magnitude cut-off to the population age (Salaris 2009).

We close our theoretical analysis presenting two additional tests about our derived WD ages. First, we have recalculated the BaSTI WD isochrones considering the WD IFMR by Kalirai et al. (2009) instead of the default IFMR employed by the BaSTI isochrones (Salaris et al. 2009). In the WD progenitor mass range typical of NGC 6819 (progenitor masses above ∼1.6 $M_\odot$), this different IFMR predicts generally slightly lower progenitor masses at fixed WD mass, compared to the BaSTI default IFMR. This implies that with the Kalirai et al. (2009) IFMR WDs of a given mass start to cool along the CS at a later time, hence they reach somewhat brighter magnitudes for a given WD isochrone age (we recall that the WD isochrone age is equal to the sum of the progenitor age plus the WD cooling age), compared to the case of the Salaris et al. (2009) IFMR. Comparisons with the observed LF show that the use of the Kalirai et al. (2009) IFMR increases the estimate of the WD age by just 40 Myr.

As a second test, we have considered the DA WD cooling tracks by Renedo et al. (2010 – their calculations for metallicity approximately half-solar, the closest to NGC 6819 metallicity in their calculations), that are completely independent from the BaSTI WD models employed here. Renedo et al. (2010) calculations follow the complete evolution of the WD progenitors through the thermal pulse phases and include the effect of CO phase separation upon crystallization, like BaSTI WD models. The CO stratification and envelope thickness of Renedo et al. models (as well as the model input physics) are slightly different from BaSTI models, but the cooling times down to the luminosities of the bottom of the observed CS of NGC6819 are similar. From their calculations, the match of the cut-off of the observed LF provide an age older by ∼100 Myr compared to the age determined with our reference BaSTI WD models.

4 PROPER MOTIONS

In principle, a mild contamination from field objects, might also affect the shape of the WD LF, but again, it cannot change the magnitude location of the sharp drop-off in the WD LF. In this

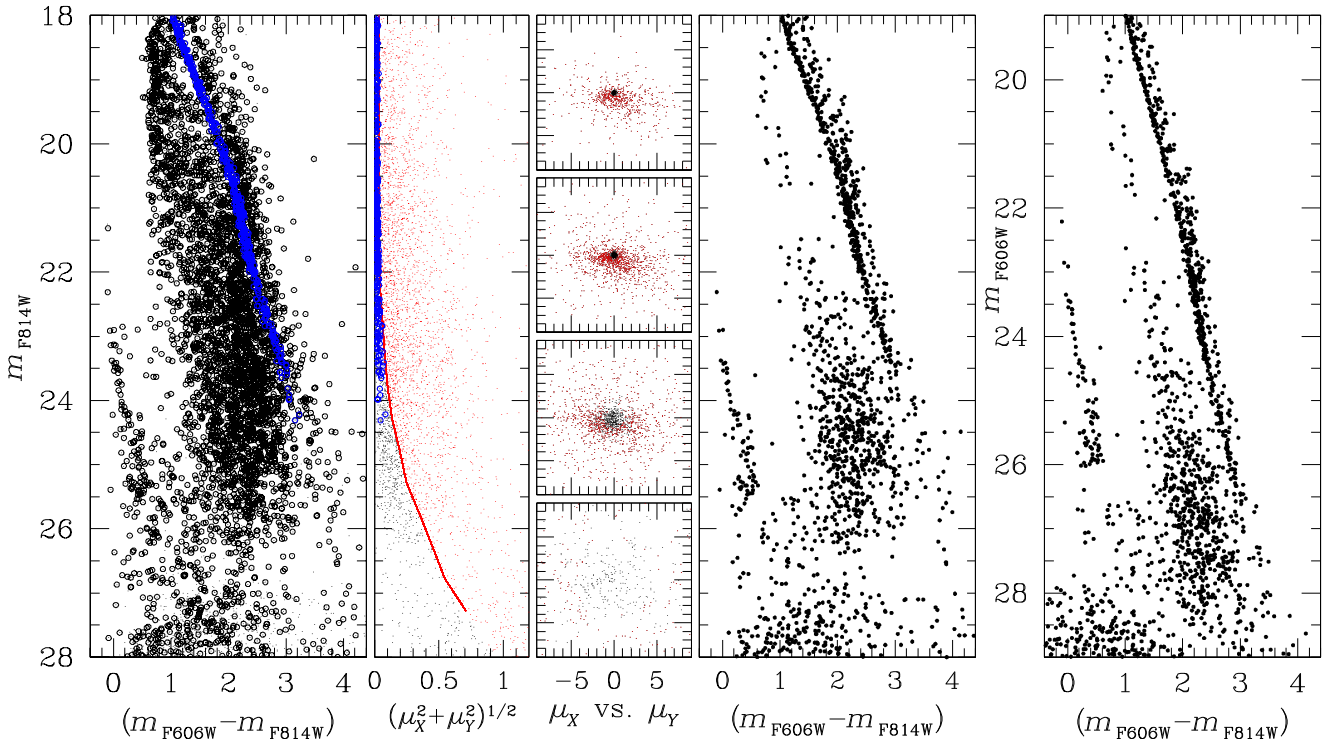

Figure 5. Left: ($m_{F606W} - m_{F814W}$) versus m_{F814W} CMD of stars in panel (b) of Fig. 2 (small dots). The stars for which it was possible to compute a proper motion are highlighted with empty circles. Blue dots mark the MS stars used to compute the interepoch transformations necessary to compute proper motions. Second panel from left: m_{F814W} versus total proper motions in mas yr^{-1} relative to the mean proper motion of the cluster. Errors increase towards fainter magnitudes. The red line isolate the objects that have member-like motions (black) from field objects (red dots). Third panels from left: are vector point diagrams for those stars in four magnitude bins. Right-hand panels: resulting decontaminated CMDs. Note how the sharp drop of the WD CS results even clearer than in the left-hand panel.

section, we use proper motions to strengthen the cluster membership of the observed stars in the expected CMD location of the WD CS.

Proper motions were determined by means of the techniques described in Bedin et al. (2003, 2006, 2009, 2014). We used the deep exposures in F814W collected in 2009 October as first epoch, while we used the F814W exposures taken in 2012 October as second epoch. The proper motions are calculated as the displacement between the average positions between the two epochs, divided by the time base-line (about 3 years), and finally multiplied by the pixel scale. We assumed a WFC3/UVIS pixel scale of 39.773 mas pixel^{-1} (Bellini, Anderson & Bedin 2011). As the proper motions signals are a function of the F814W magnitude only, we plot proper motions properties as a function of this magnitude, rather than F606W.

Unfortunately, the cluster has a proper motion that is not significantly different from the bulk of the field objects, and our precision is too low for an accurate discrimination between field objects and cluster members, especially at the magnitudes of the faintest WDs. Furthermore, proper motions are not available for all sources, with an incompleteness that is hard to assess quantitatively (and reliably); the precision of the derived proper motions is also heterogeneous across the sample.

Even though we cannot do quantitative work with the proper motions, we can still use them in a qualitative way to confirm: (i) the truncation of the WD LF, (ii) the observed shape of the end of the WD CS (as the stars having proper motions are also the ones with the best photometry), and (iii) the goodness of the employed isochrones (how well they reproduce the blue-turn).

The left-hand panel of Fig. 5 shows as small dots all stars in panel (c) of Fig. 2, but this time plotting the colour *versus* m_{F814W} instead of *versus* m_{F606W}. Stars for which it was possible to estimate a proper motion are highlighted with open circles. Only members along the MS were used to define the transformations between the two epochs, and they are marked in blue. In the second panel, we show for this subsample of stars the magnitudes of the proper motions versus m_{F814W}. Cluster members should have a dispersion of the order of $\sim$1 km s^{-1}, which at a distance of $\sim$2.4 kpc would correspond to a proper motion internal dispersion of less than 0.1 mas yr^{-1}, making them an ideal almost-fixed reference frame. For this reason, our zeroes of the motion will coincide with the cluster bulk motion.

It can be seen that at high-signal-to-noise ratio, cluster stars have a sharp proper motion distribution which is consistent with a few times 0.1 mas yr^{-1}, but embedded in the middle of a cloud of field objects, mainly thin disc and thick disc stars [NGC 6819 is at $(l,b) \simeq (74^\circ,8^\circ)$]. Note the increasing size of random errors with decreasing signal-to-noise ratio.

In order to separate members from non-members, we used the results of the AS test illustrated in (f_3 and f_4) and derive the 1D σ as the 68.27th percentile of the added−recovered positions for each coordinate at different magnitude steps. The red line marks the 2.5σ level.

Non-members, to the right of the red line, are marked in red. In the third panel from left, using the same symbols, we show the vector-point diagrams (in mas yr^{-1}) for four different magnitude bins (m_{F606W} = 18–20.5, 20.5–23, 23–25.5 and 25.5–28). The CMDs that result from the cleaning criterion of the second panel are shown in the rightmost panels of the same figure, using both filters. No matter how tight the circle is, even at the brightest magnitudes, there will always be field objects that accidentally have the same motions of

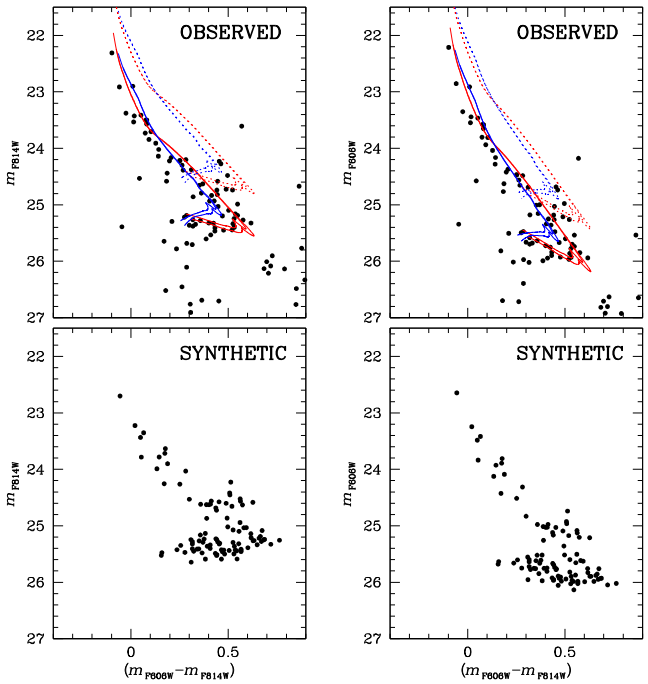

Figure 6. A zoom-in of the decontaminated CMDs in Fig. 5 centred on the WD CS, with colour versus m_{F814W} in left-hand panels and versus m_{F606W} in the right-hand panel. The top panels display the observed CMDs, with overimposed the WD isochrones employed in Fig. 3 (solid lines: DA in red, DB in blue). We also display, as dotted lines, the same isochrones but 0.75 mag brighter, to mark approximately the magnitude and colour range covered by a population of unresolved WD+WD binaries. The bottom panels display the synthetic CMDs corresponding to the reference LF shown as a solid line in panel (b) of Fig. 4 (see Section 3 for details) with approximately the same number of stars of the decontaminated CMDs (see Section 3 for details).

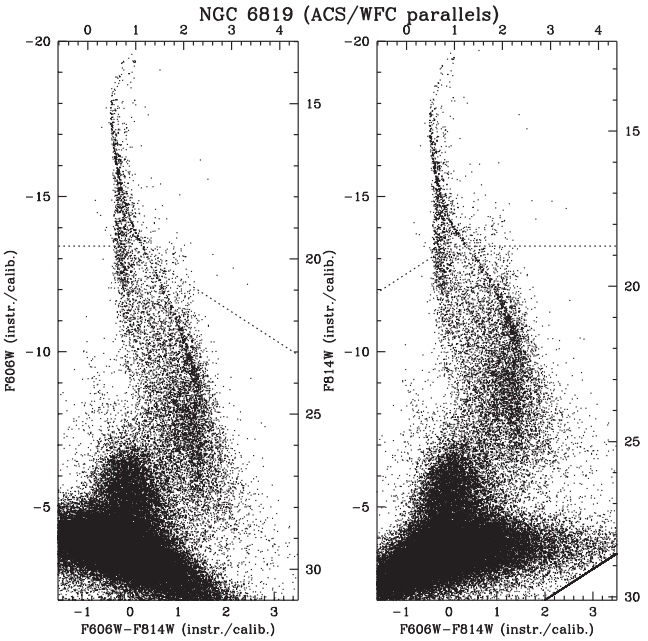

Figure 7. CMDs obtained from the ACS/WFC parallel fields shown in the bottom-right panel of Fig. 1. The bottom and left axes display instrumental magnitudes, while the top and right the calibrated ones. Dashed lines indicate the level where saturation sets-in. Note that it is possible to recover photometry for saturated stars up to about 3.5 mag above these limits (see Gilliland 2004 for details), but not enough to observe the MS TO stars reliably.

NGC 6819 members. Thankfully, the WDs of NGC 6819 occupy a low-contamination region of the CMD, were few blue faint stars exist, field WDs and blue compact galaxies both being generally significantly fainter (Bedin et al. 2009).

Although affected by low completeness, it seems even more clear that the sharp drop at $m_{F606W} \simeq 26.05$ (i.e. $m_{F814W} \simeq 25.6$) in Fig. 2(c) is real and that the few objects along the continuation of the WD CS at $m_{F606W} \sim 27$ (i.e. $m_{F814W} \simeq 26$) are most likely field WDs or background unresolved galaxies.

Finally, in Fig. 6 we show the CMDs of the decontaminated WD CS. Although very incomplete, these contain the best-measured WDs in our sample, offering a higher photometric-precision version of the complete sample used to derive the WD LF. Indeed, the shape of the observed blue-turn here appears to be significant, and most importantly consistent with the shape of the WD DA isochrones (indicated in red) and with the synthetic CMDs for the reference LF of panel (b) in Fig. 4. Very interestingly, the synthetic CMDs show around $m_{F606W} \sim 25$ and $(m_{F606W} - m_{F814W}) \sim 0.5$ a feature caused by the unresolved WD+WD binaries included in the simulation (see Section 3 for details), that corresponds to the end of the DA CS shifted 0.75 mag brighter (see upper panels of the same figure). The observed CMDs exhibit a very similar feature located at the same magnitude and colour, hinting at the presence of a small fraction of unresolved WD+WD systems, as suggested also by the fit of the LF (see Section 3).

A future paper (involving other team members) will deal with the absolute motions of NGC 6819 with respect to background galaxies in order to compute the cluster Galactic orbit using as input the sources in the catalogue described in the next section. (Similar to the study of the orbit of NGC 6791 done in Bedin et al. 2006.)

5 ELECTRONIC MATERIAL: WFC3/UVIS AND ACS/WFC

The catalogue is available electronically in this journal (and also under request to the first author). In the catalogue, Column (1) contains the running number; Columns (2) and (3) give the J2000 equatorial coordinates in decimal degrees for the epoch J2000.0, while Columns (4) and (5) provide the pixel coordinates x and y in a distortion-corrected reference frame. Columns (6) to (11) give photometric data, i.e. m_{F606W} and m_{F814W} magnitudes and their errors. If photometry in a specific band is not available, a flag equal to 99.999 is set for the magnitude and 0.999 – for the error. In Fig. 7, we show the CMDs obtained from the unselected catalogue of the ACS/WFC parallel fields, which we have not analysed and used in this article. For ACS/WFC, we provide the entire list of all detections, these still include blends and other artefacts. For the case of WFC3/UVIS main catalogue, we also provide the subset of the selected stars as shown in Fig. 2 and a WD flag. We also provide the photometry from short exposures.

The stack images shown in the bottom panels of Fig. 1 provide a high-resolution representation of the astronomical scene that enables us to examine the region around each source. Indeed, the pixel-based representation of the composite data set provides a nice objective cross-check on the catalogue-based representations, which is a product of our subjective finding and selection criteria. The stacked images are 20 000 × 20 000 for UVIS (and 24 000 × 24 000 for WFC) supersampled pixels (by a factor of 2, i.e. 20 mas pixel^{-1} for UVIS, 25 mas pixel^{-1} for WFC). We have included in the header

of the image, as World Coordinate System keywords, our absolute astrometric solution based on the 2MASS point source catalogue. As part of the material of this article, we also electronically release these astrometrized stacked images.

6 CONCLUSIONS

We have used *HST* to observe the WD sequence in NGC 6819, a near solar-metallicity old open cluster within the *Kepler* mission field of view. By means of our photometry and completeness tests, we have determined the LF of the cluster WD CS, which exhibits a sharp drop at $m_{\rm F606W} = 26.050 \pm 0.075$, and a shape consistent with theoretical predictions for a canonical cluster CS.

Isochrone fits to the cluster MS have provided $E(B - V) = 0.17 \pm 0.01$, $(m - M)_0 = 11.88 \pm 0.11$, and a MS TO age $t_{\rm MS\,TO} = 2.25 \pm 0.30$ Gyr. These distances and ages are in agreement with independent constraints from eclipsing binary and asteroseismological analyses.

We have reassessed the robustness of the WD LF cut-off magnitude as age indicator and determined an age of 2.25 ± 0.20 Gyr from the CS, completely consistent with the age of 2.25 ± 0.30 Gyr obtained from the MS TO. We have tested the effect of a different IFMR on our WD ages, obtaining an age larger by just 40 Myr when using the Kalirai et al. (2009) IFMR instead of our reference Salaris et al. (2009) IFMR. We have also employed the completely independent set of WD calculations by Renedo et al. (2010) and determined an age older by just 100 Myr compared to the result with our reference WD models.

This agreement between WD and MS TO ages is in line with the results we obtained in our previous studies of NGC 2158 and M 67, two open clusters spanning the age range between ∼2 and ∼4 Gyr.

As a by-product of this work we release, in electronic format, both the catalogue of all the detected sources and the atlases of the region (in two filters), contained in the *Kepler* field.

ACKNOWLEDGEMENTS

JA and IRK acknowledge support from STScI grant GO-11688 and GO-12669. PB was supported in part by the NSERC Canada and by the Fund FRQ-NT (Québec).

REFERENCES

Anderson J., Bedin L. R., 2010, PASP, 122, 1035
Anderson J. et al., 2008, AJ, 135, 2055
Anthony-Twarog B. J., Deliyannis C. P., Twarog B. A., 2014, AJ, 148, 51
Bedin L. R., Piotto G., King I. R., Anderson J., 2003, AJ, 126, 247
Bedin L. R., Cassisi S., Castelli F., Piotto G., Anderson J., Salaris M., Momany Y., Pietrinferni A., 2005a, MNRAS, 357, 1038
Bedin L. R., Salaris M., Piotto G., King I. R., Anderson J., Cassisi S., Momany Y., 2005b, ApJ, 624, L45
Bedin L. R., Piotto G., Carraro G., King I. R., Anderson J., 2006, A&A, 460, L27
Bedin L. R., King I. R., Anderson J., Piotto G., Salaris M., Cassisi S., Serenelli A., 2008a, ApJ, 678, 1279
Bedin L. R., Salaris M., Piotto G., Cassisi S., Milone A. P., Anderson J., King I. R., 2008b, ApJ, 679, L29
Bedin L. R., Salaris M., Piotto G., Anderson J., King I. R., Cassisi S., 2009, ApJ, 697, 965
Bedin L. R., Salaris M., King I. R., Piotto G., Anderson J., Cassisi S., 2010, ApJ, 708, L32
Bedin L. R., Ruiz-Lapuente P., González Hernández J. I., Canal R., Filippenko A. V., Mendez J., 2014, MNRAS, 439, 354
Bellini A. et al., 2010, A&A, 513, 50
Bellini A., Anderson J., Bedin L. R., 2011, PASP, 123, 622
Bragaglia A. et al., 2001, AJ, 121, 327
Bravo E., Isern J., Labay J., Canal R., 1992, A&A, 257, 534
Brogaard K. et al., 2012, A&A, 543, A106
Deloye C. J., Bildsten L., 2002, ApJ, 580, 1077
García-Berro E., Hernanz M., Mochkovitch R., Isern J., 1988, Nature, 333, 642
García-Berro E. et al., 2010, Nature, 465, 194
García-Berro E., Torres S., Renedo I., Camacho J., Althaus L. G., Córsico A. H., Salaris M., Isern J., 2011, A&A, 533, A31
Gilliland R., 2004, ACS Instrument Science Report 2004-01. STScI, Baltimore
Hansen B. M. S., 1998, Nature, 394, 860
Hansen B. M. S. et al., 2004, ApJS, 155, 551
Hansen B. M. S. et al., 2007, ApJ, 671, 380
Jeffries M. W., Jr, et al ., 2013, AJ, 146, 58
Kalirai J. S., Bergeron P., Hansen B. M. S., Kelson D. D., Reitzel D. B., Rich R. M., Richer H. B., 2007, ApJ, 671, 748
Kalirai J. S., Saul D. D., Richer H. B., Bergeron P., Catelan M., Hansen B. M. S., Rich R. M., 2009, ApJ, 705, 408
Milliman K. E., Mathieu R. D., Geller A. M., Gosnell N. M., Meibom S., Platais I. E., 2014, AJ, 148, 38
Milone A. P. et al., 2012, ApJ, 744, 58
Oswalt T. D., Smith J. A., Wood M. A., Hintzen P. M., 1996, Nature, 382, 692
Pietrinferni A., Cassisi S., Salaris M., Castelli F., 2004, ApJ, 612, 168
Podsiadlowski P., 2014, in González Martínez-País I., Shahbaz T., Casares Velázquez J., eds, Accretion Processes in Astrophysics. Cambridge Univ. Press, Cambridge, p. 45
Renedo I., Althaus L. G., Miller B. M. M., Romero A. D., Córsico A. H., Rohrmann R. D., García-Berro E., 2010, ApJ, 717, 183
Richer H. B., Fahlman G. G., Rosvick J., Ibata R., 1998, ApJ, 504, L91
Salaris M., 2009, in Mamajek E. E., Soderblom D. R., Wyse R. F. G., eds, Proc. IAU Symp. 258, The Ages of Stars. Cambridge Univ. Press, Cambridge, p. 258
Salaris M., Serenelli A., Weiss A., Miller Bertolami M., 2009, ApJ, 692, 1013
Salaris M., Cassisi S., Pietrinferni A., Kowalski P. M., Isern J., 2010, ApJ, 716, 1241
Sandquist E. L. et al., 2013, ApJ, 762, 58
von Hippel T., 2005, ApJ, 622, 565
Williams K. A., 2004, ApJ, 601, 1067
Winget D. E., Hansen C. J., Liebert J., van Horn H. M., Fontaine G., Nather R. E., Kepler S. O., Lamb D. Q., 1987, ApJ, 315, L77
Wu T., Li Y., Hekker S., 2014, ApJ, 786, 10
Yang S.-C., Sarajedini A., Deliyannis C. P., Sarrazine A. R., Kim S. C., Kyeong J., 2013, ApJ, 762, 3

SUPPORTING INFORMATION

Additional Supporting Information may be found in the online version of this article:

As part of this article the authors release four catalogs, and four astrometrized stacked images, described in Section 5. (http://mnras.oxfordjournals.org/lookup/suppl/doi:10.1093/mnras/stv069/-/DC1).

Please note: Oxford University Press are not responsible for the content or functionality of any supporting materials supplied by the authors. Any queries (other than missing material) should be directed to the corresponding author for the article.

This paper has been typeset from a TEX/LATEX file prepared by the author.